THE JOURNAL OF CHEMICAL PHYSICS **134**, 134306 (2011)

Two- and three-body photodissociation dynamics of diiodobromide (I_2Br^-) anion

Paul E. Crider, Aaron W. Harrison, and Daniel M. Neumark[a)]
Department of Chemistry, University of California, Berkeley, California 94720, USA and Chemical Sciences Division, Lawrence Berkeley National Laboratory, Berkeley, California 94720, USA

(Received 12 November 2010; accepted 9 March 2011; published online 6 April 2011)

The photodissociation of gas-phase I_2Br^- was investigated using fast beam photofragment translational spectroscopy. Anions were photodissociated from 300 to 270 nm (4.13–4.59 eV) and the recoiling photofragments were detected in coincidence by a time- and position-sensitive detector. Both two- and three-body channels were observed throughout the energy range probed. Analysis of the two-body dissociation showed evidence for four distinct channels: $Br^- + I_2$, $I^- + IBr$, $Br + I_2^-$, and $I + IBr^-$. In three-body dissociation, $Br(^2P_{3/2}) + I(^2P_{3/2}) + I^-$ and $Br^- + I(^2P_{3/2}) + I(^2P_{3/2})$ were produced primarily from a concerted decay mechanism. A sequential decay mechanism was also observed and attributed to $Br^-(^1S) + I_2(B\,^3\Pi_{0u}^+)$ followed by predissociation of $I_2(B)$. © *2011 American Institute of Physics*. [doi:10.1063/1.3571474]

I. INTRODUCTION

For many years, trihalide anions have attracted interest as model systems for studying fundamental physical processes in chemistry.[1] Their formation by the freezing of sea salt components has been proposed as a possible source of ozone depletion in polar atmospheres.[2,3] The $I_3{}^-$ anion is the best known of the trihalides. It readily produces I_2^- upon photolysis in solution-phase chemistry[4–6] and can be used as a redox mediator in dye-sensitized solar cells.[7] It has served as a benchmark for comparing dynamics in solution and in the gas phase, with UV photodissociation experiments in the two media showing vibrational coherences in the I_2^- photoproduct that indicated considerably more vibrational excitation in the gas phase.[8–10] Gas phase experiments have also characterized the energetics[11,12] and primary photochemistry of I_3^- with emphasis on elucidating the branching ratios among the available two- and three-body product channels.[13–16] In this paper, the photodissociation dynamics of I_2Br^-, which is isovalent to I_3^- but noncentrosymmetric, are investigated with the goal of understanding how the two- and three-body dissociation dynamics of a trihalide change when its symmetry is broken.

Compared to I_3^-, the heteronuclear trihalides are relatively unexplored. These species are linear, and the most stable isomer has the least electronegative atom occupying the center position in the molecule.[17,18] Landrum *et al.*[19] performed discrete Fourier transform (DFT) calculations on I_2X^- species and indeed found that linear structures with an I atom in the center are more stable than other arrangements, as more of the negative charge resides on the terminal atoms. Ogawa *et al.*[20] carried out electronic structure calculations to determine structure and dissociation energies of heteronuclear trihalides in the gas phase and in solution. Sanov *et al.*[21] performed DFT calculations at the *m*PW1PW level to determine the structure and dissociation energies of $BrICl^-$ and IBr_2^-, finding that the isomers with the I atom in the center are favored by around 0.5 eV.

Solution-phase absorption spectra for various trihalides have been analyzed,[22,23] as well as Raman and infrared spectra.[24] Popov *et al.*[23] found two broad absorption maxima for I_2Br^- in acetonitrile at 351 and 280 nm, analogous to the two bands in the I_3^- absorption spectrum at 360 and 290 nm.[5] Later work by Eyal *et al.*[25] measured the maximum of the upper band of I_2Br^- to be 270 nm. In time-resolved experiments, Gershgoren *et al.*[9] found enhanced vibrational coherences in the I_2^- product from the photodissociation I_2Br^- compared to I_3^-, an effect attributed to the noncentrosymmetic structure of I_2Br^-.

In the gas phase, Sanov *et al.*[21] performed femtosecond pump-probe experiments to study the time-resolved photodissociation dynamics of $BrICl^-$ and IBr_2^- around 400 nm (3.0–3.5 eV). For $BrICl^-$, only IBr^- and ICl^- fragments were detected, while only IBr^- fragments were detected for IBr_2^-, suggesting that their ion source produced only the most stable isomer in which the I atom occupies the center position. They also detected vibrational coherences in the IBr^- and ICl^- photofragments indicating higher average vibrational excitation than in the I_2^- formed from I_3^-.[8] Mabbs *et al.*[26] used femtosecond anion photoelectron spectroscopy to investigate the I^- channel in the 388 nm (3.2 eV) photodissociation of I_2Br^-, observing the time-resolved evolution of the excess-electron wave function from the I_2Br^- molecular orbital to the atomic orbital of I^-. In addition, they established a lower bound of 4.0 eV for the electron affinity (EA) of neutral I_2Br. Crawford *et al.*[27] investigated the collision-induced dissociation of I_2Br^-, finding approximately equal yields of I^- and Br^- over a laboratory collision energy range of 20–50 eV.

In this paper, we report results on I_2Br^- photodissociation from the upper absorption band using fast beam photofragment translational spectroscopy. Our experiments characterize both two-body and three-body dissociation

---

[a)] Author to whom correspondence should be addressed. Electronic mail: dneumark@berkeley.edu.

0021-9606/2011/134(13)/134306/12/$30.00

channels. These experiments provide a basis for comparison of the photodissociation dynamics of the triiodide anion and a noncentrosymmetric analog. Our two-body photofragment translational energy distributions suggest that I_2, I_2^-, IBr, and IBr^- are formed in highly vibrationally excited states, in accordance with other trihalides.[8–10,13–16,21,28–33] We obtain bond dissociation energies and the heat of formation of I_2Br^- from our three-body translational energy distributions, and extract detailed information on the three-body dissociation mechanism by means of Dalitz plot analysis.[34]

II. EXPERIMENT

The photodissociation experiments were performed on our fast beam photofragment translational spectrometer. This apparatus has been described in detail previously.[35–37] I_2Br^- ions were produced by flowing 5% methyl bromide (Sigma, 95%) in Ar (~20 psi) over IBr crystals (Sigma, 98%) at room temperature. The carrier gas with precursor was supersonically expanded through a piezoelectric pulsed valve operating at 60 Hz. The gas expansion occurred across a pulsed discharge (~0.5 kV) and was intersected with a 1 keV electron beam generated by an electron gun. The resulting anions were accelerated to a laboratory-frame beam energy of 8 keV and mass-selected using a Bakker time-of-flight mass spectrometer.[38,39] The two isotopes of bromine occur in approximately equal abundance and the $I_2{}^{79}Br^-$ (333 amu) isotopolog was chosen for the experiments reported here.

After exiting the source region, the ion packet intersected a laser pulse from a XeCl excimer-pumped (Lambda Physik LPX 210, 308 nm) tunable dye laser (Lambda Physik FL 3002). The wavelengths used in this experiment ranged from 300 to 270 nm (4.13–4.59 eV). Recoiling photofragments were detected 2.15 m downstream of the dissociation region by a time- and position-sensitive coincidence imaging detector based on the design by Zajfman *et al*.[40] This detector consisted of three 75 mm diameter imaging quality microchannel plates (MCPs) arranged in a Z-stack configuration and coupled to a phosphor screen. Spots appearing on the phosphor screen corresponded to the impinging photofragments; the resulting image was split by a dichroic beam splitter to a 4 × 4 multianode PMT array for timing information and a charge-coupled device camera via an image intensifier for position information. Undissociated parent ions and intact photodetached neutrals were blocked by a 5 mm diameter beam block positioned before the detector. The current setup detects both anions and neutral photofragments that have cleared the beam block.

The coincidence arrival times and positions were used to infer the masses and the center-of-mass (COM) translational energy release of the photofragments for each photodissociation event. In two-body dissociation events, the angle of recoil θ was also obtained. In three-body events, the COM momenta of all three fragments were determined. This information was used to construct COM translational energy distributions and, for three-body events, Dalitz plots[34] describing the momentum partitioning among the fragments. Owing to the presence of the beam block and the finite diameter of the detector, detection efficiency was limited for events of certain recoil geometries. These considerations were accounted for by normalizing the raw distributions with a detector acceptance function (DAF) (Ref. 41) to obtain the $P(E_T)$ distributions. In the work presented here, only two-body events were DAF-corrected; three-body events are presented as raw $N(E_T)$ distributions. In the absence of a DAF, the three-body distributions are expected to be biased toward high E_T events.

III. THEORETICAL METHODS

Ab initio calculations of dissociation energies of $IIBr^-$ and $IBrI^-$ were performed using coupled-cluster theory with single and double excitations and treating triple excitations perturbatively [CCSD(T)]. The aug-cc-PVnZ-PP bases were used for $n = 4$, 5, and the computed values were extrapolated to the complete basis limit.[42] Further details on these calculations are provided in the supplementary material. As a benchmark system, calculations were initially performed on the well-characterized I_3^- anion. The calculated dissociation energy of 1.349 eV is in remarkable agreement with the experimental value of 1.31 eV.[11] This methodology was then applied to the two isomers of I_2Br^-. For isomer 1 ($IIBr^-$), these calculations predict nearly identical values of 1.42 and 1.43 eV for dissociation into $Br^- + I_2$ and $I^- + IBr$, respectively. Isomer 2, $IBrI^-$, was found to lie 0.35 eV above $IIBr^-$, in accordance with the general rule for trihalide structures. This energy difference was reflected in the lower dissociation energy of isomer 2 of approximately 1.08 eV. Additional energetics are tabulated in the supplementary material.[76] All calculations were carried out using the MOLPRO 2009 suite of programs.[43]

From either $D_0(I_2-Br^-)$ or $D_0(BrI-I^-)$, one can derive the energetics of all possible two- and three-body dissociation channels from I_2Br^-. These are listed in Table I. Note that the values in Table I for channel 1A, $Br^-(^1S) + I_2(X^1\Sigma_g^+)$, and channel 2A, $I^-(^1S) + IBr(X^1\Sigma^+)$, upon which all the other energies are based, are very close to the calculated values of D_e but were actually determined from this experiment, as discussed in Sec. V. The other dissociation energies were then determined by combining these energies with previously established experimental values for the spin–orbit coupling constants for iodine and bromine, the dissociation energies of I_2,[44] I_2^-,[45] IBr,[46] and IBr^-,[47] the electron affinities of Br, I, and I_2,[48] and the term energies of the A and B states of I_2 (Refs. 49 and 50) and IBr.[51–54]

IV. EXPERIMENTAL RESULTS

The photodissociation of I_2Br^- was investigated at photon energies between 4.13 and 4.59 eV (300 – 270 nm), all of which lie within its upper absorption band.[23] Photofragment mass ratios were determined to identify the product channels. Figure 1(a) plots photofragment mass ratio distributions as a function of photon energy and normalized by area. Three mass ratios, 0.31:1, 0.62:1, and 1:1, were observed in the two-body data, corresponding to three distinct two-body mass channels. One three-body mass channel was also observed. Figure 1(b) is a sample plot ($h\nu = 4.28$ eV) of the photofragment mass distribution for this channel, with a feature at

TABLE I. List of product channels organized by fragment masses in amu. Dissociation energies for each channel are given in electron volts (eV).

	Mass channel (amu)	Product channel	D_0 (eV)	Equation label
I_2Br^-	79 + 254	$Br^-(^1S) + I_2(X^1\Sigma_g^+)$	1.44	1A
		$Br(^2P_{3/2}) + I_2^-(X^2\Sigma_u^+)$	2.28	1B
		$Br^*(^2P_{1/2}) + I_2^-(X^2\Sigma_u^+)$	2.74	1C
		$Br^-(^1S) + I_2(A^3\Pi_{1u})$	2.79	1D
		$Br^-(^1S) + I_2(B^3\Pi_{0u}^+)$	3.39	1E
		$Br(^2P_{3/2}) + I_2(X^1\Sigma_g^+) + e^-$	4.80	DPD1[a]
	127 + 206	$I^-(^1S) + IBr(X^1\Sigma^+)$	1.47	2A
		$I(^2P_{3/2}) + IBr^-(X^2\Sigma_{1/2}^+)$	2.02	2B
		$I^-(^1S) + IBr(A\prime^3\Pi_2)$	2.88	2C
		$I(^2P_{1/2}) + IBr^-(X^2\Sigma_{1/2}^+)$	2.96	2D
		$I^-(^1S) + IBr(A^3\Pi_1)$	2.99	2E
		$I^-(^1S) + IBr(B^3\Pi_0^+)$	3.47	2F
		$I^-(^2P_{3/2}) + IBr(X^1\Sigma^+) + e^-$	4.53	DPD2[a]
	79 + 127 + 127	$Br^-(^1S) + I(^2P_{3/2}) + I(^2P_{3/2})$	2.98	3A
		$Br^-(^2P_{3/2}) + I^-(^1S) + I(^2P_{3/2})$	3.29	3B
		$Br^*(^2P_{1/2}) + I^-(^1S) + I(^2P_{3/2})$	3.74	3C
		$Br^-(^1S) + I^*(^2P_{1/2}) + I(^2P_{3/2})$	3.92	3D

[a] DPD, dissociative photodetachment.

79 amu and one at 127 amu with about twice the intensity, corresponding to one bromine and two iodine fragments, respectively.

Figure 1 shows that four product mass channels result from the dissociation of I_2Br^-: channel 1, with mass ratio 0.31:1, corresponding to $Br^- + I_2$ or $Br + I_2^-$, channel 2, with mass ratio 0.62:1, corresponding to $I^- + IBr$ or $I + IBr^-$, channel 3, corresponding to three-body dissociation as determined by the coincident detection of three fragments, and channel 4, corresponding to three-body dissociation where two fragments with a 1:1 mass ratio are detected, suggesting events in which the bromine fragment is blocked and two iodine fragments strike the detector. Note that "fragment" refers universally to charged and neutral species; for example, "iodine fragment" indicates only a fragment of mass 127 amu, regardless of charge.

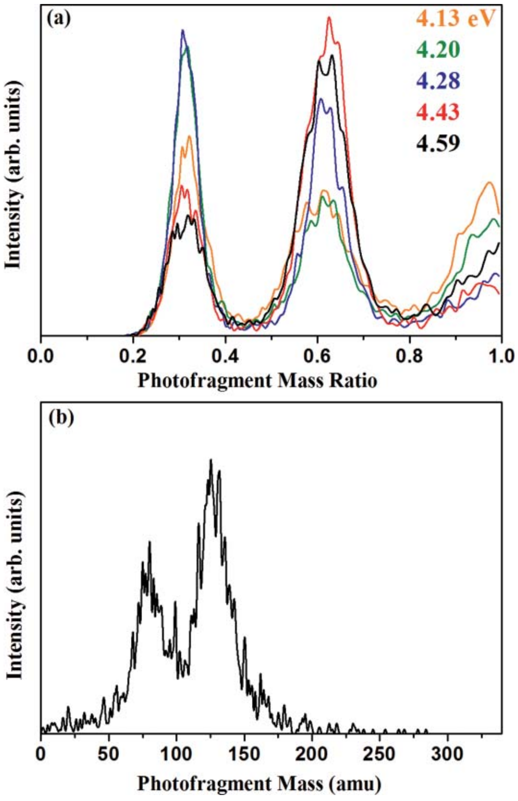

FIG. 1. (a) Photofragment mass ratio of two-fragment valid events following excitation of I_2Br^- at photon energies of 4.13–4.59 eV and (b) three-body photofragment mass distribution following excitation at $h\nu = 4.28$ eV.

Figures 2 and 3 show two-body photofragment $P(E_T)$ distributions for mass channels 1 and 2, respectively. In each of these figures, the $P(E_T)$ distributions observed from all five photon energies are presented. In Figs. 2 and 3(a), each $P(E_T)$ distribution has been shifted to higher kinetic energy by $\Delta E_{h\nu}$, defined as the difference in energy between the dissociation photon and a 4.59 eV photon (the highest energy photon used). In this scheme, features corresponding to the same fragment internal energy line up vertically, thereby facilitating peak assignment. The scaled energy axis in Fig. 3(b) is discussed in Sec. V. Figures 2 and 3 also show brackets labeled with possible product channels that indicate the range of E_T possible for each channel, from $E_T^{\min}$ to $E_T^{\max}$. $E_T^{\max}$ values are determined from the dissociation values given in Table I. $E_T^{\min}$ values are determined from the well depth of the diatomic product, corresponding to the maximum possible internal excitation, beyond which three-body dissociation occurs. In both figures, qualitative changes are evident in the features of the $P(E_T)$ distributions as photon energy increases, indicating that different product channels become populated.

We also extract anisotropy parameters,[55] $[\beta(E_T)]$, for each two-body mass channel. These distributions are determined by fitting the DAF-corrected $P(E_T,\theta)$ distribution to the equation

$$P(E_T,\theta) = P(E_T)[1 + \beta(E_T)P_2(\cos\theta)], \tag{1}$$

where θ is the angle between the electric field vector of the laser pulse and the recoil vector of the photofragments and

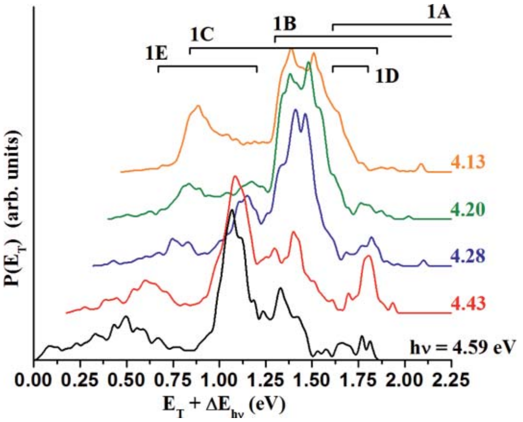

FIG. 2. Photofragment translational energy distributions for two-body dissociation of I_2Br^- into 79 and 254 amu fragments. $P(E_T)$ distributions are shifted to higher E_T by 4.59 eV ($h\nu$). The allowed translational energies for channels 1A–1E are bracketed.

$P_2(\cos\theta)$ is the second Legendre polynomial. $\beta(E_T)$ ranges from –1, indicating a $\sin^2\theta$ distribution, to 2 for a $\cos^2\theta$ distribution. The measured values of $\beta(E_T)$ for the major dissociation pathways are reported in the supplemental material.[76]

In Fig. 4, the raw (not DAF-corrected) $N(E_T)$ distributions for three-body dissociation are presented. Because I_2Br^- is a triatomic molecule, all available energy must be deposited in translation or electronic excitation. Indeed, we observe sharp peaks at all five photon energies that appear at successively higher E_T as the photon energy is increased, reflecting the additional energy available for translation. The peaks rise abruptly and then tail off toward higher kinetic energy, reflecting the internal energy distribution of the anions.

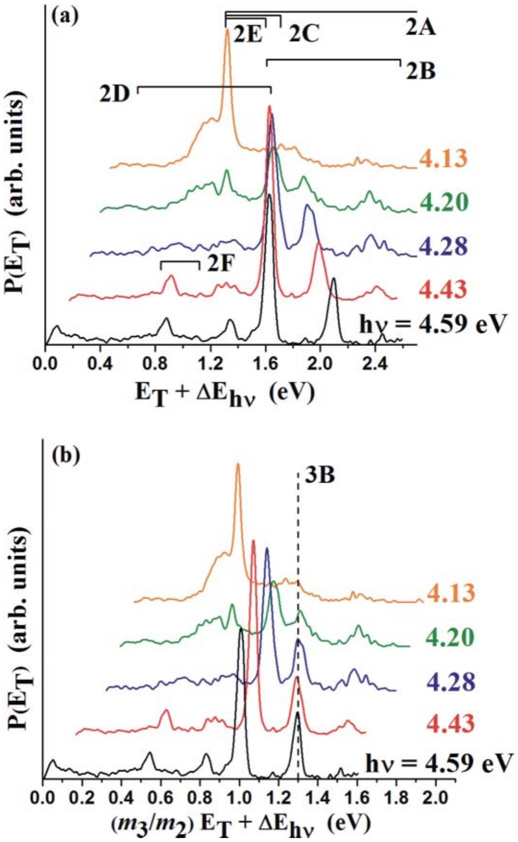

FIG. 3. (a) Photofragment translational energy distributions for two-body dissociation of I_2Br^- into 127 and 206 amu fragments. $P(E_T)$ distributions are shifted to higher E_T by 4.59 eV ($h\nu$). The allowed translational energies for channels 2A–2F are bracketed. (b) $P(E_T)$ distributions scaled by mass ratio of IBr to IIBr (see text) and shifted by 4.59 eV ($h\nu$). The dotted line is drawn at the expected E_T for channel 3B.

V. ANALYSIS

At every wavelength studied, both two-body mass channels are in evidence. The accessible energy ranges for the various product channels overlap as indicated by the brackets in Figs. 2 and 3. As a result, assignments of features in the $P(E_T)$ distributions to specific channels can be ambiguous. We generally favor assignments in which the feature in question falls off sharply near either $E_T^{\max}$ or $E_T^{\min}$ for a particular channel, especially if this falloff is observed at multiple photon energies. In cases where a two-body channel falls off at $E_T^{\min}$, one expects to observe the corresponding three-body channel from dissociation of the diatomic fragment, so the presence or absence of a three-body channel can help assign the two-body feature.

A. Two-body dissociation: Br + I_2 fragments

In Fig. 2, the $P(E_T)$ distributions for mass channel 1 ($Br^- + I_2$ or $Br + I_2^-$) are plotted against $E_T + \Delta E_{h\nu}$. Beginning at 4.13 eV, two broad features are apparent. The most prominent feature extends from ∼1.25 to ∼1.60 eV. This feature lies within the energetic limits of channels 1B, $Br(^2P_{3/2}) + I_2^-(X^2\Sigma_u^+)$, and 1C, $Br^*(^2P_{1/2}) + I_2^-(X^2\Sigma_u^+)$. However, since it drops off abruptly below $E_T^{\min}$ for channel 1B, we favor its assignment to this channel, indicating that I_2^- is produced in highly vibrationally excited states extending up to its dissociation asymptote. A similar feature is observed at each photon energy, though it is diminished at 4.43 and 4.59 eV.

Moving to the $P(E_T)$ distribution at 4.28 eV, a feature is evident between 1.00 and 1.25 eV. A similar feature is observed with greater intensity at 4.43 and 4.59 eV. This feature falls within the energy ranges of channels 1C and 1E and occurs just below $E_T^{\max}$of channel 1E, $Br^- + I_2(B\,^3\Pi_{0u}^+)$. While both pathways may contribute, the sharp decrease in intensity above $E_T^{\max}$ for channel 1E suggests assignment to that channel. This assignment is corroborated by evidence for predissociation of $I_2(B^3\Pi_{0u}^+)$ presented below in our discussion of three-body dynamics. Peaking near $E_T^{\max}$ indicates the electronically excited $I_2(B)$ fragments are produced with little internal excitation, in contrast to the vibrationally excited diatomic fragments associated with the other features. Another feature appears in the 4.28 eV $P(E_T)$ distribution near $E_T + \Delta E_{h\nu} \approx 1.8$ eV and becomes more intense at 4.43 eV. This feature falls well within the energy limits of channels 1A and 1B; given its falloff near $E_T^{\min}$ for channel 1A, we assign it to this pathway, leading again to vibrationally excited diatomic fragments.

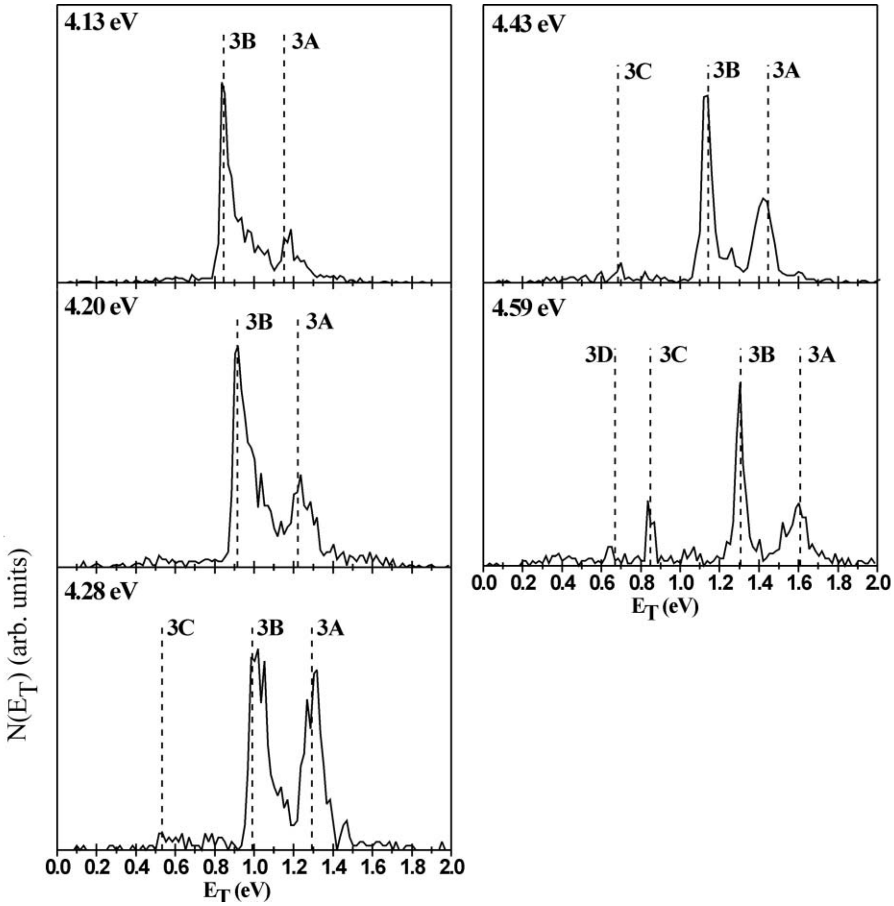

FIG. 4. Photofragment translational energy distributions for three-body dissociation of I_2Br^- upon excitation by photon energies of 4.13–4.59 eV. The expected kinetic energy release for channels 3A–3D is indicated by dashed lines.

The final feature to consider in Fig. 2 is the broad, low energy feature present at all dissociation energies. Assignment of this feature is problematic. Unlike all the other features in Fig. 2, it shifts toward lower $E_T + \Delta E_{h\nu}$ with increasing photon energy, and in fact remains at constant energy when plotted as a function of E_T. This dependence could indicate dissociative photodetachment (DPD1) to $\mathrm{Br} + \mathrm{I}_2 + e^-$, with the excess photon energy going into electron kinetic energy, but as shown in Table I, the threshold for DPD1 is too high for such an assignment. Considering other two body-channels, this feature could be a combination of channels 1C and 1E from 4.13 to 4.28 eV, with the $I_2{}^-$ and I_2, respectively, highly excited in both channels.

The feature in question clearly lies beyond channel 1E at 4.43 and 4.59 eV. Some signal at these higher energies could be from Br and $\mathrm{I}_2^-(^2\Pi_{u,1/2})$, which should fall around $E_T + \Delta E_{h\nu} > 0.36$ eV. However, this state of I_2^- is calculated to be very weakly bound (0.08 – 0.19 eV);[56–58] it would have been bound by at least 0.3 eV to account for the energy range of this feature at 4.43 and 4.59 eV. Other possible excited states of neutral I_2 are unlikely given that the minimum energy asymptote for channel 1E represents the formation of I + I*, for which $E_T^{\min}$ is already too high. Therefore, this feature would have to originate from a state that not only correlates to I* + I* but also has a sufficiently deep well to access the observed translational energies (ΔE_{SO} of iodine is 0.943 eV); to our knowledge no such state is known for I_2.

B. Two-body dissociation: I + IBr fragments

$P(E_T)$ distributions for mass channel 2, I + IBr fragments, are presented in Fig. 3(a). The distributions are plotted against $E_T + \Delta E_{h\nu}$ as in Fig. 2. At 4.13 eV, there is a sharp feature near 1.3 eV. This feature occurs near $E_T^{\min}$ for channels 2A, 2C, and 2E, corresponding to $\mathrm{I}^-(^1S)$ and IBr in its ground electronic state ($X^1\Sigma^+$) or its first two excited states. This feature diminishes significantly at higher photon energies. We thus assign it to dissociation via one or more of these three channels, with the IBr fragment highly vibrationally excited regardless of its electronic state.

Also at 4.13 eV, a feature appears around $E_T + \Delta E_{h\nu} \approx 1.15$ eV, overlapping the other feature. This feature falls within the limits of channel 2D, $\mathrm{I}^*(^2P_{1/2}) + \mathrm{IBr}^-(X^2\Sigma^+_{1/2})$. It peaks near 50% of $E_T^{\min}$, indicating IBr^- fragments are produced in a range of vibrational levels. A similar feature is also apparent at $E_{h\nu} = 4.20$ eV, though diminished, and no evidence for this channel is observed at higher photon energies.

At all photon energies ≥ 4.20 eV, the most intense feature in the $P(E_T)$ distributions is a sharp peak near $E_T + \Delta E_{h\nu}$

$\approx$ 1.65 eV; this peak is not seen at all at 4.13 eV. While it appears within the energetic limits of channel 2A and arguably 2C, this feature drops to nearly zero intensity below $E_T^{\min}$ of channel 2B, $\mathrm{I}(^2P_{3/2})$ + $\mathrm{IBr}^-(X^2\Sigma^+_{1/2})$, leading us to assign it to this channel. The close alignment with $E_T^{\min}$ once again indicates the diatomic fragment is produced near its dissociation asymptote.

At 4.43 and 4.59 eV, a small feature is evident at $E_T + \Delta E_{h\nu} \approx 0.85$ eV. This feature falls within the relatively small energy range corresponding to channel 2F, $\mathrm{I}^-(^1S)$ + $\mathrm{IBr}(B^3\Pi^+_0)$. There is a low intensity feature observed at each dissociation wavelength around $E_T + \Delta E_{h\nu} \approx 2.35$ eV, which appears to be low internal energy photoproducts from either channel 2A or 2B. Finally, at 4.59 eV, the small feature below $E_T = 0.1$ is attributed to dissociative photodetachment.

Figure 3(a) also shows a feature that shifts smoothly from $E_T + \Delta E_{h\nu} \approx 1.85$ eV at 4.13–2.10 eV by 4.59 eV, appearing as a distinct, sharp peak at photon energies ≥4.20 eV. While this feature falls well within the energetic bounds of several dissociation pathways, such as channel 2B, there is no clear correspondence to any one channel. Furthermore, it is surprising that the diatomic products would be produced with less internal energy as the photon energy increases. We resolve this riddle by considering the possible presence of three-body dissociation from IIBr^- in which only the two terminal atoms are detected and the central I atom hits the beam block, giving a mass ratio of 79:127 = 0.622. This mass ratio is coincidentally nearly identical to mass channel 2 (127:206 = 0.617), and would thus lead to two-body signal in Fig. 3.

Since the mass of the parent anion is assumed in our analysis, three-body dissociation events with only two detected fragments will be treated as having a higher (and incorrect) reduced mass, leading to $P(E_T)$ distributions artificially shifted to higher kinetic energy. This effect can be corrected by scaling the apparent two-fragment energy $E_{2\text{frag}}$ to the ratio of masses,

$$E_{3\text{body}} = \frac{m_{3\text{body}}}{m_{2\text{frag}}} E_{2\text{frag}} = 0.619 E_{2\text{frag}}, \qquad (2)$$

where $m_{3\text{body}} = m_{\mathrm{Br}} + m_{\mathrm{I}}$, $m_{2\text{frag}} = m_{\mathrm{Br}} + 2m_{\mathrm{I}}$, and $E_{3\text{body}}$ is the corrected three-body translational energy. Figure 3(b) shows the same distributions as in Fig. 3(a) plotted against the scaled energy 0.619 $(E_T + E_{h\nu})$. The features in question all line up in this plot at a scaled energy of 1.306 eV, which corresponds to the expected kinetic energy release from channel 3B at 4.59 eV photon energy, as discussed further in Sec. V C.

C. Three-body dissociation

In the three-body photofragment $N(E_T)$ distributions presented in Fig. 4, the peaks can be readily assigned by comparing the peak spacings to the energetics of channels 3A–3D listed in Table I. At each wavelength, the dominant three-body channel is 3B, dissociation to $\mathrm{Br} + \mathrm{I} + \mathrm{I}^-$. Also present in each panel of Fig. 4 is a feature from the lower energy channel 3A, $\mathrm{Br}^- + \mathrm{I} + \mathrm{I}$. In the $N(E_T)$ distributions at 4.28 eV and higher, a small feature from channel 3C is in evidence, corresponding to dissociation into spin–orbit excited $\mathrm{Br}^*(^2P_{1/2})$ and I_3^-. There is some evidence for channel 3D, leading to $\mathrm{Br}^- + \mathrm{I} + \mathrm{I}^*$, at 4.59 eV. The vertical lines in all four three-body channels in Fig. 4 are drawn assuming the maximum in the peak assigned to channel 3B corresponds to the translational energy release from photodissociation of ground state anions. This value is used in Sec. V D to extract the bond dissociation energy of $\mathrm{I_2Br}^-$. We attribute the high kinetic energy tails on the peaks in Fig. 4 to internally excited anions in the molecular beam, from which we estimate the internal energy to be 50–100 meV.

Additional insight into the three-body dissociation dynamics is provided by the Dalitz plots[34,59,60] in Figs. 5 and 6 that show momentum partitioning among the three fragments for peaks 3A and 3B, respectively. Each side of the triangle is an axis corresponding to the fraction of the square of the momentum, $f_i = p_i^2/\Sigma p_j^2$, of one fragment. Each point corresponds to a three-body event and is constrained by conservation of energy to fall within the equilateral triangle and by conservation of momentum to fall within an inscribed circle. Points at the periphery of this circle correspond to events in which the three momentum vectors are collinear, while those closer to the center correspond to progressively more noncollinear momenta. In each plot, the lower axis corresponds to the squared-momentum contribution of the bromine fragment, and the other two axes correspond to the iodine fragments. Because the two iodine fragments are indistinguishable in our detection scheme, the momentum partitioning exhibits twofold symmetry and can thus be plotted in half the area of the inscribed circle.[59] As the events are plotted here, I and I′ correspond to the faster and slower iodine fragments, respectively.

All of the Dalitz plots in Figs. 5 and 6 show significant intensity near the periphery of the inscribed circle, and the plots in Fig. 5 from 4.20 to 4.59 eV show a line segment along $f_{\mathrm{Br}} \approx 0.37$. The signal at the periphery is most intense at the one o'clock position. This position corresponds to events where one iodine fragment receives little momentum ($f_{\mathrm{I}} < 0.10$) and the other iodine fragment receives the bulk of the momentum balance ($f_{\mathrm{I}}' > 0.45$). This cluster of points is therefore consistent with concerted dissociation from a nearly linear configuration of IIBr^-, in which both bonds break on the time scale of vibrational motion in the anion.[61] This mechanism appears to hold for channels 3A and 3B.

Several of the Dalitz plots in Figs. 5 and 6 also show enhanced intensity along the periphery near ten o'clock. This position corresponds to events where the bromine fragment receives very little momentum ($f_{\mathrm{Br}} < 0.05$) and the iodine fragments split the momentum balance roughly equally, as would be expected from dissociation of IBrI^-. However, all of the I + IBr features in Fig. 3 can be assigned to photodissociation of IIBr^-. Moreover, assuming our calculated energetics (Sec. III) are approximately correct, three-body dissociation of IBrI^- would yield additional peaks at 0.35 eV higher energy than 3A and 3B in Fig. 4. There is clearly no such feature to the high energy side of 3A, although a peak shifted by 0.35 eV from 3B might be difficult to distinguish from 3A. It is therefore possible that there is a contribution to the ten o'clock feature in Fig. 5 (nominally channel 3A

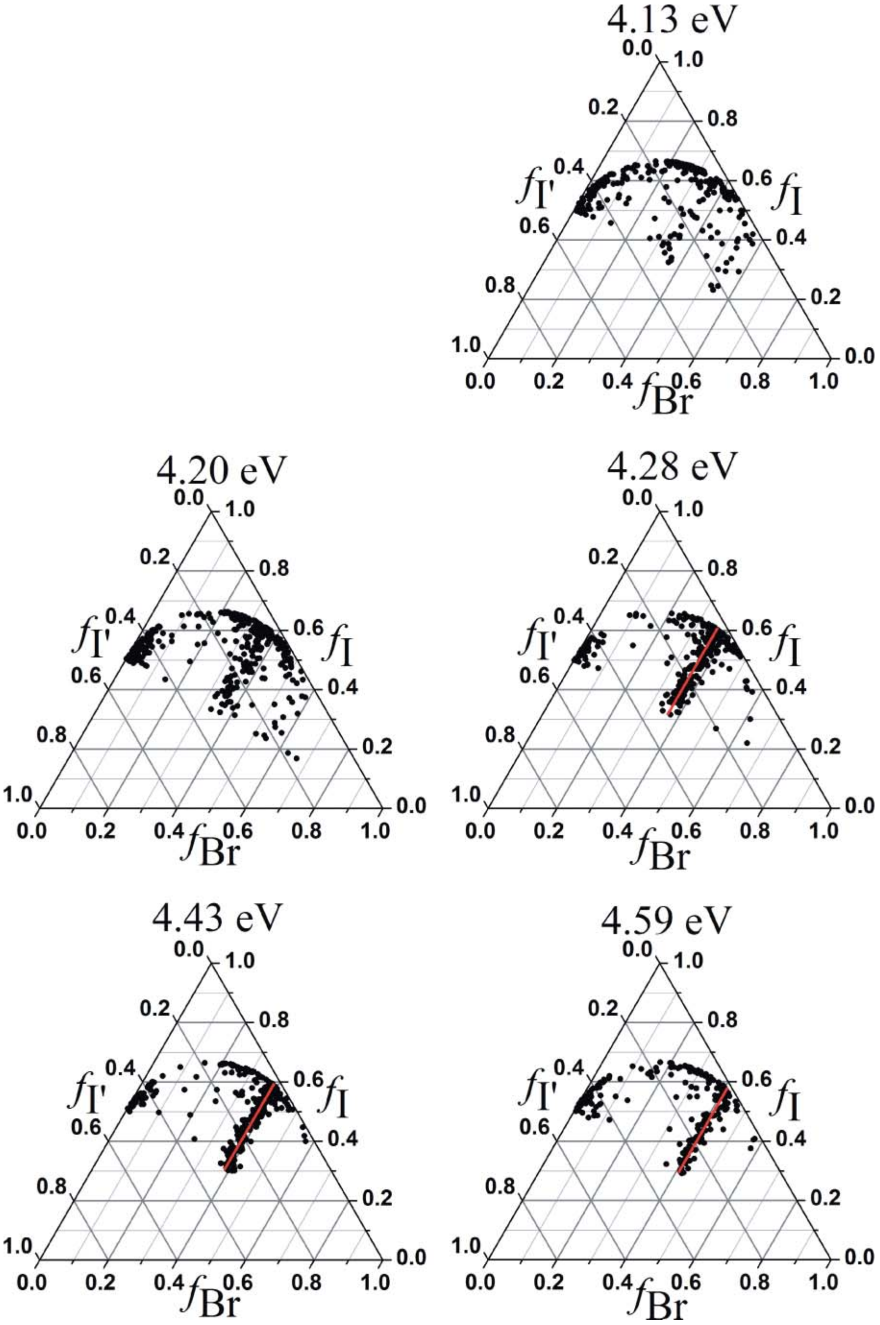

FIG. 5. Dalitz plots of momentum partitioning among the three fragments in the three-body dissociation of I_2Br^- upon excitation by photon energies of 4.13–4.59 eV. Points correspond to the 3A feature in the three-body $N(E_T)$. The red line in the plots for 4.28–4.59 eV is result of a simulation for sequential decay (see text).

from IIBr$^-$) from IBrI$^-$ dissociation via channel 3B. But the corresponding feature in Fig. 6, seen most prominently at 4.13 and 4.20 eV, cannot arise from this mechanism; there is no IBrI$^-$ three-body channel that overlaps 3B from IIBr$^-$. Hence, there must be another dissociation mechanism leading to signal in this region of the Dalitz plot. We speculate that these events arise from isomerization or large amplitude bending motion in the anion excited states prior to dissociation. Note that the calculations of Landrum *et al.*[19] showed that the 6σ LUMO is lower in energy for IBrI$^-$ than for IIBr$^-$, so population of this orbital upon excitation could play a role in isomerization.

At photon energies ≥4.20 eV in Fig. 5, the Dalitz plots show a line of points that correspond to constant bromine momentum partitioning ($f_{Br} \approx 0.37$) and randomized iodine fragment momenta. This line becomes more prominent in the plots at the three highest photon energies. This feature is a characteristic of a sequential dissociation, where the momentum of one fragment is determined independently of the other two fragment momenta.[62,63]

The kinematics of sequential dissociation can be described by a model adapted from Matsuda *et al.*[62] who used it to describe sequential fragmentation from Coulomb explosion of the benzene trication. The relevant equations are

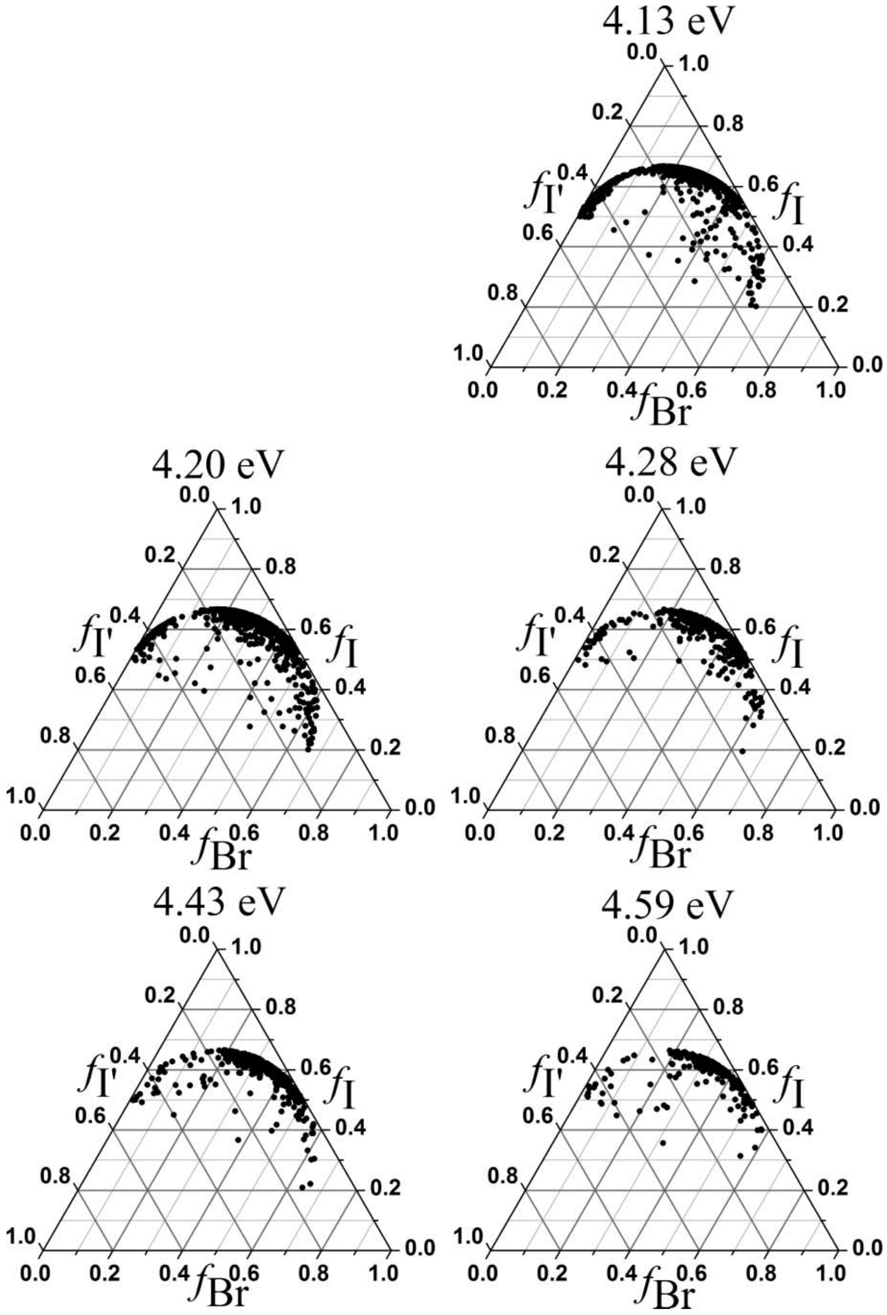

4.13 eV

4.20 eV

4.28 eV

4.43 eV

4.59 eV

FIG. 6. Dalitz plots of momentum partitioning among the three fragments in the three-body dissociation of I_2Br^- upon excitation by photon energies of 4.13–4.59 eV associated with the 3B feature in the three-body $N(E_T)$.

presented in the supplementary material.[76] Because the total E_T is well defined for each three-body decay event, it can be partitioned between the translational energy release in the first dissociation step, E_1, and that of the second dissociation step, E_2, with a single parameter ϵ, so that $E_1 = \varepsilon E_T$ and $E_2 = (1 - \varepsilon)E_T$.[63] The results of plotting momenta over all decay angles in the Dalitz plot and adjusting ϵ to fit our experimental results are shown in red in Fig. 5 for 4.28–4.59 eV, where the constant f_{Br} feature was clearly present. The resulting values of E_1 and ε for each photon energy are shown in Table II. We find that as the photon energy increases, E_1 increases as a fraction of total E_T. This is consistent with a sequential mechanism where the first dissociation step is immediate, and produces an atomic Br fragment and a metastable I_2 diatomic fragment which dissociates prior to detection ~30 μs after interaction with the photodissociation laser.

If some of the metastable I_2 did not dissociate on this time scale, one would expect to see a correlation between E_1 and some feature in the two-body $P(E_T)$ distribution for mass channel 1. Comparing the $E_1 + \Delta E_{h\nu}$ values given in Table II, all of which are ~1.1 eV, to the $P(E_T)$ distributions in Fig. 2, we find a clear correspondence to the feature assigned to channel 1E, $\mathrm{Br}^-(^1S) + \mathrm{I}_2(B^3\Pi^+_{0u})$, with values close to $E_T^{\max}$. We thus propose the following sequential dissociation mechanism for IIBr$^-$: upon absorption ($h\nu \geq 4.20$ eV), IIBr$^-$ is excited to an electronic surface

TABLE II. Numbers relevant for sequential dissociation for photon energies of 4.28–4.59 eV. E_T is the total energy deposited in translation. ϵ is a parameter describing the partitioning of E_T between the two dissociation steps (see text). E_1 is translational energy imparted in the first dissociation step. $E_1 + \Delta E_{h\nu}$ adjusts for the difference between photon energies.

$h\nu$	E_T	E	E_1	$E_1 + \Delta E_{h\nu}$
4.28	1.28	0.63	0.81	1.13
4.43	1.43	0.66	0.94	1.10
4.59	1.6	0.69	1.10	1.10

TABLE III. Branching fractions for two- and three-body dissociation of I_2Br^-.

Photon energy (eV)	Two body	Three body
4.13	0.62	0.38
4.20	0.58	0.42
4.28	0.65	0.35
4.43	0.62	0.38
4.59	0.65	0.35

correlating to $Br^-(^1S) + I_2(B^3\Pi^+_{0u})$ products; some fraction of the metastable $I_2(B^3\Pi^+_{0u})$ fragments then undergoes electronic predissociation via repulsive surfaces correlating to ground state I atoms.

D. Thermodynamic quantities

The dissociation energy of I_2Br^- can be directly obtained from the three-body $N(E_T)$ distributions in Fig. 4, taking the peak of the sharp 3B feature, $E^{3B}_{T,\text{peak}}$, as our reference point. $D_0(I^- - IBr)$ is then obtained by

$$D_0(I^- - IBr) = h\nu - E^{3B}_{T,\text{peak}} - D_0(I - Br), \tag{3}$$

where $D_0(I - Br) = 1.8181 \pm 0.0001$ eV, taken from the literature.[64,65] We find $D_0(I^- - IBr)$ to be 1.469 ± 0.01 eV, in good agreement with our calculated value of $D_e = 1.44$ eV. Similarly, using the known electron affinities[48] of I and Br, we report $D_0(Br^- - I_2) = 1.442 \pm 0.01$ eV, which is comparable to our calculated value of 1.42 eV. These results, both experimental and theoretical, differ by less than 0.2 eV from the bond energies calculated by Ogawa *et al.*[20] who found $D_0(Br^- - I_2) = D_0(I^- - IBr) = 1.30$ eV and those of Landrum *et al.*[19] who calculated a bond energy of $D_0(I^- - IBr) = 1.59$ eV.

With our bond dissociation energies, the 0 K heat of formation, $\Delta_f H(I_2Br^-_{(g)})$ can be determined by (4),

$$\Delta_f H(I_2Br^-_{(g)}) = \Delta_f H(I_{2(g)}) + \Delta_f H(Br^-_{(g)}) - D_0(Br^- - I_2), \tag{4}$$

where $\Delta_f H(I_{2(g)}) = 65.50 \pm 0.08$ kJ mol^{-1} (Ref. 66) and $\Delta_f H(Br^-_{(g)}) = -206.60 \pm 0.12$ kJ mol^{-1} were determined from $\Delta_f H(Br_{(g)}) = 117.93 \pm 0.12$ kJ mol^{-1} (Ref. 66) and its EA.[48] We find $\Delta_f H(I_2Br^-_{(g)})$ to be –2.90 ± 0.01 eV, or –280.2 ± 1 kJ mol^{-1}.

E. Branching fractions

Branching fractions between two- and three-body dissociation were obtained at all dissociation energies. However, owing to less than unit detection efficiency of an impinging particle on the MCP detector, the measured branching fractions are biased toward "two-fragment" events as these events are detected with a higher probability than "three-fragment" ones. Approximating the particle detection efficiency of the incident MCP as 0.5,[67] the measured branching ratios were appropriately corrected,[68] and these values are shown in Table III. The three-body branching ratio includes both two- and three-fragment events that were assigned to three-body dissociation with the appropriate scaling. Three-body dissociation constitutes ~35%–42% of the total fragmentations, and this fraction does not show much dependence on wavelength.

In addition, we attempted to quantify the disposal of the excess electron between the possible atomic and molecular fragments at each dissociation energy, however due to the spectral overlap of the many possible dissociation pathways for this molecule, it is very difficult to accurately determine these values. See the supplementary material for a complete tabulation of these results.[76] This analysis indicates that the most prevalent anion produced from the sum of the two- and three-body channels is I^-, similar to the observations of Mabbs *et al.*[26] following excitation to the lower energy band (3.2 eV). All possible anion products are produced at each photon energy, though I_2^- becomes a more minor channel at the highest photon energies.

VI. DISCUSSION

These experiments demonstrate the rich photodissociation dynamics of I_2Br^- from the upper absorption band, which involve multiple two- and three-body channels. These translational energy distributions are similar to those from the lower absorption band of I_3^-, where the two-body channels blended seamlessly into the corresponding three-body channels,[14] and suggest that two- and three-body dissociation occur via the same dynamical process. Specifically, at 4.13 eV, the $Br(^2P_{3/2}) + I_2^-(X^2\Sigma_u^+)$ and $I^-(^1S) + IBr$ channels (1B, 2A, 2B, and 2C) all correlate to channel 3B in the limit of maximum internal excitation of the diatomic fragment, and the two-body $P(E_T)$ distributions all feature sharp falloffs at $E_T^{\min}$. In this dynamical picture, $IIBr^-$ is excited to a manifold of electronic excited states, and dissociation occurs along a repulsive surface via the stretching coordinate, resulting in three-body dissociation or an atom and a vibrationally excited diatomic when one bond fails to cleave. This mechanism is consistent with the Dalitz plot of channel 3B in Fig. 6, which indicates that dissociation proceeds primarily by a concerted mechanism where both bonds break before the diatomic product has a chance to rotate, resulting mainly in collinear dissociation events at the perimeter of the inscribed circle.

The high degree of vibrational excitation in the photoproducts is consistent with the large differences in bond lengths between the ground state anions and the diatomic products. For example, our calculated value for the ground state anion bond length, $R_{\mathrm{eq}}(\mathrm{II}-\mathrm{Br}^-) = 2.748$ Å, is significantly longer than that of ground state IBr (2.469 Å).[64,65] A simple Franck–Condon picture[69] of the photodissociation dynamics would predict high vibrational excitation of the IBr fragment, in agreement with our observations. Similarly, $R_{eq}(\mathrm{BrI}-\mathrm{I}^-) = 2.936$ Å differs significantly from the I–I bond length in both ground state I_2^- (3.205 Å; Ref. 45) and neutral I_2 (2.666 Å).[70]

However, in contrast to the other two-body dissociation pathways, both the two-body $P(E_T)$ distributions and the sequential three-body decay suggest that $\mathrm{I}_2(B)$ formed in dissociation has little vibrational excitation, as this feature peaks near E_T^{max} in the two-body translational energy distributions and predissociation of $\mathrm{I}_2(B)$ occurs more efficiently in lower vibrational energy levels. Also, as the photon energy increases, the additional energy is almost entirely funneled into kinetic energy release in the primary dissociation, E_1. This observation can again be reconciled with the aid of a simple Franck–Condon picture noting that the equilibrium I–I bond length in the trihalide (~2.94 Å) is very close to that of the B-state of I_2 (~3.02 Å). It is also possible that the initial dissociation occurs following promotion to a directly repulsive surface such that nearly all of the energy is converted into translation with little vibrational energy deposition in the diatomic fragment.

Upon absorption at 4.13 eV, dissociation preferentially proceeds along channels producing $\mathrm{I}_2^-(X^2\Sigma_u^+)$ or I^-, with some contribution from channels 1A or 1D, producing Br^-. In each case, the $P(E_T)$ distribution includes events at the edge of E_T^{min}, reflecting maximum internal excitation of the diatomic fragment. Upon dissociation into three atoms, the excess electron is most likely to leave with an I atom. This is also true at 4.20 eV, but excitation at 4.20 eV produces different two-body dynamics in mass channel 2. The two-body pathway producing $\mathrm{I}^-(^1S) + \mathrm{IBr}$ products (from channels 2A, 2C, or 2E) has diminished and a feature corresponding to three-body dissociation where only an iodine and a bromine are detected has grown in intensity in Fig. 3(b). Three-body dissociation of IIBr^- where only the terminal atoms are detected must come from events where the central iodine atom has struck the beam block in front of the detector. Given the asymmetry of the molecule, a concerted three-body dissociation would impart nonzero momentum to the central atom, allowing it to pass by the beam block. For a central I fragment to strike the beam block, some events corresponding to very little or zero iodine momentum must occur. Similar events, where all three fragments are detected, should be observable in the Dalitz plots in Fig. 6. Such events are evident at $f_{I'} = 0$.

At 4.28 eV, $\mathrm{I}(^2P_{3/2}) + \mathrm{IBr}^-(X^2\Sigma_{1/2}^+)$ is a dominant channel (2B). As $\mathrm{IBr}^-(X^2\Sigma_{1/2}^+)$ correlates to Br^- and ground state $\mathrm{I}(^2P_{3/2})$, the feature assigned to channel 2B in the $P(E_T)$ distribution also extends through E_T^{min} into the three-body $P(E_T)$ distribution for channel 3A. This reflects concerted dissociation similar to the case of channel 3B discussed above. Neutral I_2 is also observed, in its ground electronic state as well as in the $(B^3\Pi_{0u}^+)$ state. As $h\nu$ is increased from 4.28 to 4.43 eV and further to 4.59 eV, signal from $\mathrm{Br}(^2P_{3/2}) + \mathrm{I}_2^-(X^2\Sigma_u^+)$ (channel 1B) diminishes while signal from channel 1E increases. This increase in intensity correlates with a stronger line of constant f_{Br} in the Dalitz plots in Fig. 5, consistent with an increasing population of predissociating $\mathrm{I}_2(B^3\Pi_{0u}^+)$. In addition to the growing contribution from channel 1E, excitation by higher energy photons results in the population of several minor channels, reflecting a greater number of electronic excited states being accessed. Channel 2F, producing $\mathrm{I}^-(^1S)$ and $\mathrm{IBr}(B^3\Pi_0^+)$ fragments, appears at $h\nu \geq 4.28$ eV; this coincides with the appearance of channel 3C, producing $\mathrm{Br}^*(^2P_{1/2})$.

The three-body photodissociation dynamics of 4.28–4.59 eV are of particular interest, specifically the line of constant f_{Br} hinted in the 4.20 eV Dalitz plot for channel 3A and clearly present at the three highest photon energies. As discussed in Sec. V C, this line indicates a sequential three-body decay, where the first bond breaks, leaving a metastable fragment, $\mathrm{I}_2(B^3\Pi_{0u}^+)$ in this case, destined later to undergo a second dissociation step. $\mathrm{I}_2(B^3\Pi_{0u}^+)$ is known to electronically predissociate via coupling to the $\mathrm{I}_2(B''^1\Pi_{1u})$ repulsive curve, leading to ground state iodine atoms.[71–74] The predissociation occurs on the order of microsecond (Ref. 75) and is dependent on the (ν, J) levels populated, with Franck–Condon density (FCD) maxima occurring at $\nu = 5$ and $\nu = 25$, and a minimum at $\nu = 14$. Fluorescence from the B-X transition also occurs to some extent at all vibrational levels, with maxima around $\nu < 5$ and $\nu = 25$ and a global minimum near the dissociation asymptote.[75] The ratio of the rate of predissociation to that of fluorescence has a minimum at $\nu = 14$.[73] The average E_1 of 1.11 eV (Table II) corresponds to $\mathrm{I}_2(B)$ with $\nu \approx 6$, which is close to the FCD maximum of $\nu = 5$. Both radiative decay and predissociation are possible at the low ν levels observed in our experiment. The two-body events producing $\mathrm{I}_2(B)$ fragments have likely undergone radiative decay, which occurs on a similar timescale of 0.4–7 μs,[75] consistent with our detection ~30 μs after absorption.

It is interesting that no evidence for similar sequential three-body dissociation has been observed in I_3^-, either in our group[13,14] or others.[15,16] While we only tentatively assigned an $\mathrm{I}^-(^1S) + \mathrm{I}_2(B^3\Pi_{0u}^+)$ product channel, Nakanishi[15] assigned the channel at nearly the same photon energy (4.28 and 4.27 eV, respectively) with a branching fraction of 0.11. Although $\mathrm{Br}^-(^1S) + \mathrm{I}_2(B^3\Pi_{0u}^+)$ in the present study is a more significant channel than $\mathrm{I}^-(^1S) + \mathrm{I}_2(B^3\Pi_{0u}^+)$ in the I_3^- system, evidence for sequential dissociation is quite distinctive in the Dalitz analysis used by us for both ions. We infer from this that any $\mathrm{I}_2(B^3\Pi_{0u}^+)$ fragments produced in the photodissociation of I_3^- do not later undergo electronic predissociation. As there is significant overlap in the energetics of the $\mathrm{I}^-(^1S) + \mathrm{I}_2(B^3\Pi_{0u}^+)$ channel and $\mathrm{I}^*(^2P_{1/2}) + \mathrm{I}_2^-(X^2\Sigma_u^+)$, it is difficult to infer the vibrational distribution of $\mathrm{I}_2(B)$ in the two-body $P(E_T)$ distributions. It is possible that any $\mathrm{I}_2(B)$ fragments detected in those experiments were produced in vibrational levels around $\nu = 14$ or significantly higher than $\nu = 25$ (the second predissociation peak).[75] These $\mathrm{I}_2(B)$ fragments likely undergo fluorescence before detection, as fluorescence at any vibrational level is on the order of a few μs and thus consistent with our detection timeline (>30 μs in the I_3^- experiment).

VII. CONCLUSIONS

We have investigated the photodissociation dynamics of $IIBr^-$ using a fast beam photofragment translational spectrometer. The anions were photodissociated at five energies between 4.13 and 4.59 eV. Fragments from both two- and three-body events were collected and analyzed using a time- and position-coincidence imaging detector. At each dissociation wavelength, photofragment mass ratios and translational energy distributions were measured and three-body Dalitz plots were constructed.

Both two- and three-body dissociation channels were detected at each wavelength employed, with three-body dissociation from $IIBr^-$ constituting about a third of events detected at each photon energy. Some shifts in $IIBr^-$ photodissociation dynamics are observed between 4.13 and 4.28–4.59 eV. While two-body channels producing $I_2^-(X^2\Sigma_u^+)$ and $IBr(X^1\Sigma^+)$ channels dominate at the lowest photon energy, both channels diminish at the higher excitation energies and are eclipsed by $Br^-(^1S) + I_2(B^3\Pi_{0u}^+)$ and $I(^2P_{3/2}) + IBr^-(X^2\Sigma_{1/2}^+)$ pathways. The two-body $I^-(^1S)$ channel appears to be replaced by three-body dissociation upon higher excitation.

Among the three-body channels, $I^-(^1S) + I(^2P_{3/2}) + Br(^2P_{3/2})$ was the preferred pathway at every wavelength, although $I(^2P_{3/2}) + I(^2P_{3/2}) + Br^-(^1S)$ was always present. Analysis of momentum disposal in three-body events using Dalitz plots shows both channels occur by concerted bond cleavage, under some influence of bending motions. In addition, the Dalitz plots reveal that $I(^2P_{3/2}) + I(^2P_{3/2}) + Br^-(^1S)$ also occurs by sequential dissociation via primary generation of $Br^-(^1S)$ and metastable $I_2(B^3\Pi_{0u}^+)$, which subsequently predissociates via coupling to a repulsive curve correlating to ground state products. Interestingly, there is no evidence for such sequential decay in the photodissociation of I_3^- in similar wavelength ranges.

ACKNOWLEDGMENTS

This research was supported by the Director, Office of Basic Energy Science, Chemical Sciences Division of the U.S. Department of Energy under Contract No. DE-AC02-05CH11231. The authors thank Etienne Garand for his help with the calculations.

[1] G. C. Pimentel, J. Chem. Phys. **19**, 446 (1951).
[2] P. O'Driscoll, K. Lang, N. Minogue, and J. Sodeau, J. Phys. Chem. A **110**, 4615 (2006).
[3] D. O'Sullivan and J. R. Sodeau, J. Phys. Chem. A **114**, 12208 (2010).
[4] A. Barkatt and M. Ottolenghi, Mol. Photochem. **6**, 253 (1974).
[5] L. I. Grossweiner and M. S. Matheson, J. Phys. Chem. **61**, 1089 (1957).
[6] J. C. Roy, W. H. Hamill, and R. R. Williams, J. Am. Chem. Soc. **77**, 2953 (1955).
[7] G. Boschloo and A. Hagfeldt, Acc. Chem. Res. **42**, 1819 (2009).
[8] U. Banin, A. Waldman, and S. Ruhman, J. Chem. Phys. **96**, 2416 (1992).
[9] E. Gershgoren, E. Gordon, and S. Ruhman, J. Chem. Phys. **106**, 4806 (1997).
[10] M. T. Zanni, B. J. Greenblatt, A. V. Davis, and D. M. Neumark, J. Chem. Phys. **111**, 2991 (1999).
[11] K. Do, T. P. Klein, C. A. Pommerening, and L. S. Sunderlin, J. Am. Soc. Mass Spectrom. **8**, 688 (1997).
[12] T. R. Taylor, K. R. Asmis, M. T. Zanni, and D M Neumark, J. Chem. Phys. **110**, 7607 (1999).
[13] H. Choi, R. T. Bise, A. A. Hoops, and D. M. Neumark, J. Chem. Phys. **113**, 2255 (2000).
[14] A. A. Hoops, J. R. Gascooke, A. E. Faulhaber, K. E. Kautzman, and D. M. Neumark, J. Chem. Phys. **120**, 7901 (2004).
[15] R. Nakanishi, N. Saitou, T. Ohno, S. Kowashi, S. Yabushita, and T. Nagata, J. Chem. Phys. **126**, 17 (2007).
[16] L. Zhu, K. Takahashi, M. Saeki, T. Tsukuda, and T. Nagata, Chem. Phys. Lett. **350**, 233 (2001).
[17] A. D. Walsh, J. Chem. Soc. 2266 (1953).
[18] S. D. Peyerimhoff and R. J. Buenker, J. Chem. Phys. **49**, 2473 (1968).
[19] G. A. Landrum, N. Goldberg, and R. Hoffman, J. Chem. Soc., Dalton Trans. 3605 (1997).
[20] Y. Ogawa, O. Takahashi, and O. Kikuchi, J. Mol. Struct.: THEOCHEM **429**, 187 (1998).
[21] A. Sanov, T. Sanford, L. J. Butler, J. Vala, R. Kosloff, and W. C. Lineberger, J. Phys. Chem. A **103**, 10244 (1999).
[22] W. Gabes and D. J. Stufkens, Spectrochim. Acta, Part A **30**, 1835 (1974).
[23] A. I. Popov and R. F. Swensen, J. Am. Chem. Soc. **77**, 3724 (1955).
[24] A. G. Maki and R. Forneris, Spectrochim. Acta, Part A **23**, 867 (1967).
[25] E. Eyal and A. Treinin, J. Am. Chem. Soc. **86**, 4287 (1964).
[26] R. Mabbs, K. Pichugin, E. Surber, and A. Sanov, J. Chem. Phys. **121**, 265 (2004).
[27] E. Crawford, J. S. McIndoe, and T. G. Tuck, Can. J. Chem. **84**, 1607 (2006).
[28] U. Banin, R. Kosloff, and S. Ruhman, Chem. Phys. **183**, 289 (1994).
[29] U. Banin and S. Ruhman, J. Chem. Phys. **98**, 4391 (1993).
[30] U. Banin and S Ruhman, J. Chem. Phys. **99**, 9318 (1993).
[31] I. Benjamin, U. Banin, and S. Ruhman, J. Chem. Phys. **98**, 8337 (1993).
[32] T. Kuhne, R. Kuster, and P. Vohringer, Chem. Phys. **233**, 161 (1998).
[33] T. Kuhne and P. Vohringer, J. Chem. Phys. **105**, 10788 (1996).
[34] R. H. Dalitz, Philos. Mag. **44**, 1068 (1953).
[35] R. E. Continetti, D. R. Cyr, R. B. Metz, and D. M. Neumark, Chem. Phys. Lett. **182**, 406 (1991).
[36] A. A. Hoops, J. R. Gascooke, A. E. Faulhaber, K. E. Kautzman, and D. M. Neumark, Chem. Phys. Lett. **374**, 235 (2003).
[37] A. A. Hoops, J. R. Gascooke, K. E. Kautzman, A. E. Faulhaber, and D. M. Neumark, J. Chem. Phys. **120**, 8494 (2004).
[38] J. M. B. Bakker, J. Phys. E **6**, 785 (1973).
[39] J. M. B. Bakker, J. Phys. E **7**, 364 (1974).
[40] Z. Amitay and D. Zajfman, Rev. Sci. Instrum. **68**, 1387 (1997).
[41] R. E. Continetti, D. R. Cyr, D. L. Osborn, D. J. Leahy, and D. M. Neumark, J. Chem. Phys. **99**, 2616 (1993).
[42] K. A. Peterson, B. C. Shepler, D. Figgen, and H. Stoll, J. Phys. Chem. A **110**, 13877 (2006).
[43] MOLPRO, a package of *ab initio* programs written by H.-J. Werner, P. J. Knowles, F. R. Manby *et al.*, version 2009.1.
[44] F. Martin, R. Bacis, S. Churassy, and J. Verges, J. Mol. Spectrosc. **116**, 71 (1986).
[45] M. T. Zanni, T. R. Taylor, B. J. Greenblatt, B. Soep, and D. M. Neumark, J. Chem. Phys. **107**, 7613 (1997).
[46] W. G. Brown, Phys. Rev. **42**, 0355 (1932).
[47] L. Sheps, E. M. Miller, and W. C. Lineberger, J. Chem. Phys. **131**, 8 (2009).
[48] J. C. Rienstra-Kiracofe, G. S. Tschumper, H. F. Schaefer, S. Nandi, and G. B. Ellison, Chem. Rev. **102**, 231 (2002).
[49] D. R. T. Appadoo, R. J. LeRoy, P. F. Bernath, S. Gerstenkorn, P. Luc, J. Verges, J. Sinzelle, J. Chevillard, and Y. Daignaux, J. Chem. Phys. **104**, 903 (1996).
[50] P. Luc, J. Mol. Spectrosc. **80**, 41 (1980).
[51] D. T. Radzykewycz, C. D. Littlejohn, M. B. Carter, J. O. Clevenger, J. H. Purvis, and J. Tellinghuisen, J. Mol. Spectrosc. **166**, 287 (1994).
[52] E. Wrede, S. Laubach, S. Schulenburg, A. Brown, E. R. Wouters, A. J. Orr-Ewing, and M. N. R. Ashfold, J. Chem. Phys. **114**, 2629 (2001).
[53] E. Wrede, S. Laubach, S. Schulenburg, A. J. Orr-Ewing, and M. N. R. Ashfold, Chem. Phys. Lett. **326**, 22 (2000).
[54] X. N. Zheng, M. C. Heaven, and J. Tellinghuisen, J. Mol. Spectrosc. **164**, 135 (1994).
[55] R. N. Zare, Mol. Photochem. **4**, 1 (1972).
[56] J. G. Dojahn, E. C. M. Chen, and W. E. Wentworth, J. Phys. Chem. **100**, 9649 (1996).
[57] P. E. Maslen, J. M. Papanikolas, J. Faeder, R. Parson, and S. V. Oneil, J. Chem. Phys. **101**, 5731 (1994).

[58] S. B. Sharp and G. I. Gellene, Mol. Phys. **98**, 667 (2000).
[59] D. Babikov, E. A. Gislason, M. Sizun, F. Aguillon, V. Sidis, M. Barat, J. C. Brenot, J. A. Fayeton, and Y. J. Picard, J. Chem. Phys. **116**, 4871 (2002).
[60] L. M. Wiese, O. Yenen, B. Thaden, and D. H. Jaecks, Phys. Rev. Lett. **79**, 4982 (1997).
[61] C. Maul and K. H. Gericke, Int. Rev. Phys. Chem. **16**, 1 (1997).
[62] A. Matsuda, M. Fushitani, R. A. Thomas, V. Zhaunerchyk, and A. Hishikawa, J. Phys. Chem. A **113**, 2254 (2009).
[63] J. D. Savee, J. E. Mann, and R. E. Continetti, J. Phys. Chem. A **113**, 3988 (2009).
[64] D. R. T. Appadoo, P. F. Bernath, and R. J. Leroy, Can. J. Phys. **72**, 1265 (1994).
[65] T. Yukiya, N. Nishimiya, and M. Suzuki, J. Mol. Spectrosc. **214**, 132 (2002).
[66] P. J. Linstrom and W. G. Mallard, NIS Chemistry WebBook, NIST Standard Reference Database Number 69 (National Institute of Standards and Technology, Gaithersburg, MD).
[67] M. Krems, J. Zirbel, M. Thomason, and R. D. DuBois, Rev. Sci. Instrum. **76**, 093305 (2005).
[68] J. D. Savee, J. E. Mann, and R. E. Continetti, J. Phys. Chem. A **113**, 8834 (2009).
[69] Y. B. Band and K. F. Freed, J. Chem. Phys. **67**, 1462 (1977).
[70] W. F. Howard, Jr. and L. Andrews, J. Raman Spectrosc. **2**, 447 (1974).
[71] L. Brewer and J. Tellinghuisen, J. Chem. Phys. **56**, 3929 (1972).
[72] J. Tellinghuisen, J. Chem. Phys. **57**, 2397 (1972).
[73] J. Vigue, M. Broyer, and J. C. Lehmann, J. Physique **42**, 949 (1981).
[74] E. A. Pazyuk, A. V. Stolyarov, V. I. Pupyshev, N. F. Stepanov, S. Y. Umanskii, and A. A. Buchachenko, Mol. Phys. **99**, 91 (2001).
[75] G. A. Capelle and H. P. Broida, J. Chem. Phys. **58**, 4212 (1973).
[76] See supplementary material at http://dx.doi.org/10.1063/1.3571474 for details regarding the *ab initio* calculations with a full tabulation of those results (Table SI) as well as a discussion of the kinematic modeling for sequential, three-body decay. Table SII: Beta parameters for major dissociation channels and Table SIII : Electron disposal for two- and three-body dissociation.